## ARTICLE

Check for updates

# Bivalent ligands promote endosomal trafficking of the dopamine D3 receptor-neurotensin receptor 1 heterodimer

Julian Budzinski[1], Simone Maschauer[2], Hiroyuki Kobayashi [3], Pierre Couvineau [3], Hannah Vogt[1], Peter Gmeiner [1], Anna Roggenhofer[1], Olaf Prante[2], Michel Bouvier [3✉] & Dorothee Weikert [1✉]

Bivalent ligands are composed of two pharmacophores connected by a spacer of variable size. These ligands are able to simultaneously recognize two binding sites, for example in a G protein-coupled receptor heterodimer, resulting in enhanced binding affinity. Taking advantage of previously described heterobivalent dopamine-neurotensin receptor ligands, we demonstrate specific interactions between dopamine D3 ($D_3R$) and neurotensin receptor 1 (NTSR1), two receptors with expression in overlapping brain areas that are associated with neuropsychiatric diseases and addiction. Bivalent ligand binding to $D_3R$-NTSR1 dimers results in picomolar binding affinity and high selectivity compared to the binding to monomeric receptors. Specificity of the ligands for the $D_3R$-NTSR1 receptor pair over $D_2R$-NTSR1 dimers can be achieved by a careful choice of the linker length. Bivalent ligands enhance and stabilize the receptor-receptor interaction leading to NTSR1-controlled internalization of $D_3R$ into endosomes via recruitment of β-arrestin, highlighting a potential mechanism for dimer-specific receptor trafficking and signalling.

[1] Department of Chemistry and Pharmacy, Medicinal Chemistry, Friedrich-Alexander-Universität Erlangen-Nürnberg, Erlangen, Germany. [2] Department of Nuclear Medicine, Molecular Imaging and Radiochemistry, Friedrich-Alexander-Universität Erlangen-Nürnberg, Erlangen, Germany. [3] Department of Biochemistry and Molecular Medicine, Institute for Research in Immunology and Cancer, Université de Montréal, Montreal, QC, Canada. ✉email: michel.bouvier@umontreal.ca; dorothee.weikert@fau.de

Specific interactions of class A G protein-coupled receptors (GPCRs), such as the formation of homo- or heterodimers or higher order oligomers, influence signalling properties, binding affinities, receptor trafficking or enable cross-talk[1–5] and have inspired the development of bivalent ligands[6,7]. Following the leads of studies reporting ligands that selectively engage opioid receptor dimers[8], medicinal chemists have aimed at developing bivalent ligands for different class A GPCRs[9]. Comprising two pharmacophores connected to each other by a spacer, bivalent ligands are able to simultaneously engage two distinct binding sites located in the two individual protomers of a dimer[9] (Fig. 1a). As a result of the thermodynamic advantage over the monovalent binding to either receptor, they confer higher affinities and also selectivity towards their combined recognition elements[7]. Besides the undoubted value of bivalent ligands as pharmacological tools for the study of the mechanism and functional consequences of receptor-receptor interactions, targeting GPCR dimers represents a promising therapeutic approach[10].

We have previously reported a series of bivalent ligands targeting heterodimers of dopamine D2 ($D_2R$) and neurotensin receptors 1 (NTSR1)[11]. These ligands exhibit more than 1000-fold selectivity for cells coexpressing the two receptors over cells expressing only the $D_2R$ and moderate selectivity over monomeric NTSR1.

Dopamine $D_3$ receptors ($D_3R$) share 52% sequence identity (75% identity within the transmembrane regions) with $D_2R$[12] and have been reported to be involved in multiple neuropsychiatric diseases including Schizophrenia[13], Parkinson's Disease[14], and more recently neuroinflammation[15]. Besides the expression in the nucleus accumbens and caudate putamen, $D_3R$ is highly expressed in the islands of Calleja[16,17], a brain region involved in reward seeking behaviour[18]. Importantly, $D_3R$ is upregulated in the context of various drug addictions and targeting $D_3R$ with monovalent antagonists or partial agonists is seen as a promising avenue in the context of drug abuse treatment[19–22].

NTSR1 is expressed in different areas of the central nervous system (CNS) including the hypothalamus, the basal forebrain
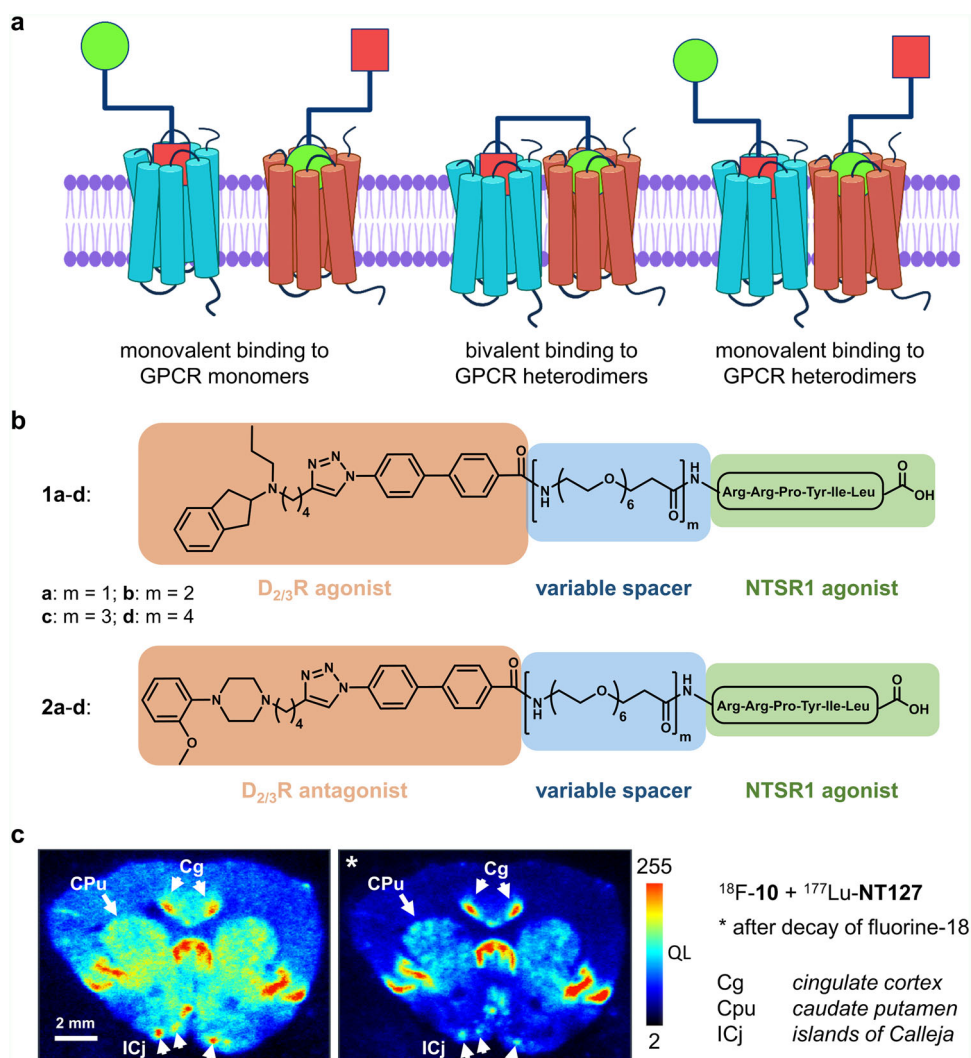


**Fig. 1 Bivalent ligands targeting heterodimers and distribution of $D_3R$ and NTSR1 in the rat CNS. a** Schematic representation of binding modes of heterobivalent ligands at dimeric or monomeric GPCRs, created with biorender.com. **b** Bivalent ligands used in the present study are composed of a dopamine receptor agonist (**1a-d**) or antagonist (**2a-d**), a linker of flexible size (m = 1-4 PEG-spacer units) and NT(8-13) as peptide NTSR1 agonist. **c** In vitro rat brain autoradiography with the $D_3R$-selective radioligand [18]F-**10**[39] and the NTSR1-selective radioligand [177]Lu-**NT127**[40] visualises the expression of $D_3R$ and NTSR1. The first image in **c** is taken directly after labelling, the second autoradiography was taken 24 h later, after complete radioactive decay of ^{18}F, showing only expression of NTSR1. Areas labelled with the white arrows indicate coexpression of $D_3R$ and NTSR1. The intensity is shown as quantum level (QL) as provided by the software Quantity One.

and the limbic system[23]. Using immunohistochemical staining, high levels of NTSR1 have also been observed in the islands of Calleja[24]. The distribution of NTSR1 reflects its role in the modulation of numerous processes, including locomotion, memory and cognition[25]. Various attempts for the clinical development of NTSR1 agonists and antagonists as neuroleptics have been made, but efforts were hampered by undesired effects including hypotension, hypothermia and motor impairment[26]. Very recently, allosteric modulation and β-arrestin biased signalling of NTSR1 have been identified as novel and promising strategies in the field of addiction therapy[27,28].

While NTSR1 is able to form homodimers[29], it also interacts with different class A GPCRs like $D_2R$ and NTSR2, resulting in heterodimer-specific ligand binding, signalling and trafficking[30–34]. Interestingly, the dopamine and neurotensin neurotransmitter systems are interconnected in the CNS and known to modulate each other[35,36]. Besides direct influences of NTSR1 on $D_2R$, negative modulation of the $D_3R$ by NTSR1 resulting in a reduced binding affinity of dopamine receptor agonists has been observed in transfected HEK293 cells[37]. Moreover, $D_3R$ and neurotensin mRNA show overlapping distribution in the rat *nucleus accumbens*[36] and neurotensin has been shown to diminish 7-OH-DPAT affinity for $D_3R$ in limbic areas of the rat brain[38]. However, bivalent ligands targeting $D_3R$-NTSR1 heterodimers have not yet been reported.

In this study, we investigate potential $D_3R$-NTSR1 heterodimer formation and examine how bivalent ligands affect the pharmacology and the trafficking of the receptors. We use our previously described bivalent $D_2R$-NTSR1 ligands **1a-d** and **2a-d** (Fig. 1b)[11] because their dopaminergic pharmacophores are not selective among members of the $D_2$-like receptor subfamily ($D_2R$, $D_3R$ and $D_4R$). Using a combination of ligand binding and bioluminescence resonance energy transfer (BRET) assays, we demonstrate that bivalent ligand binding at $D_3R$-NTSR1 heteromeric complexes occurs at very low ligand concentration and fosters the interaction of the $D_3R$ and NTSR1 protomers. Interestingly, the ligands **1a** and **2a** comprising a short linker showed selective binding to $D_3R$-NTSR1 heterodimers over $D_2R$-NTSR1 heterodimers. In contrast to stimulation with monovalent ligands, bivalent engagement of $D_3R$-NTSR1 dimers leads to internalisation of the heteromeric complex, revealing unique pharmacological properties of bivalent ligands. As ongoing research seeks to evaluate how upregulation, binding potential and function of the $D_3R$ are linked to substance abuse[20], our findings regarding altered receptor trafficking and β-arrestin recruitment properties of the $D_3R$ may pave the way towards novel therapeutic approaches, in particular since $D_3R$ and NTSR1 show expression in overlapping brain regions, even if direct evidence for their in vivo dimerization and sub-cellular colocalization remains yet to be provided.

## Results

**$D_3R$ and NTSR1 expression shows substantial overlap within rat brain.** To visualise the regional distribution of $D_3R$ and NTSR1 in the CNS, we performed in vitro rat brain autoradiography of striatal slices employing concomitant incubation with both the $D_3R$- and NTSR1-selective radioligands $^{18}$F-**10**[39] and $^{177}$Lu-**NT127**[40], respectively. The $D_3R$-selective radioligand $^{18}$F-**10** alone resulted in a labelling consistent with the known regional distribution of the $D_3R$ in the rat brain[41], including caudate putamen (CPu), nucleus accumbens (NAc), cingulate cortex (Cg) and the islands of Calleja (ICj) (Supplementary Fig. 1a). Using the selective NTSR1 radioligand $^{177}$Lu-**NT127**, high levels of NTSR1-binding sites were found in the rhinal sulcus (SR), cingulate cortex (Cg), medial septum (MS) and the islands of Calleja (ICj) and low to moderate density of binding sites in the

nucleus accumbens (Supplementary Fig. 1b), confirming the reported NTSR1 distribution in rat brain as determined by autoradiography with [$^3$H]SR142948A and immunohistochemical staining of the NTSR1[24,42]. Coincubation of rat brain slices with both radioligands showed the sum of NTSR1 and $D_3R$-binding sites, as depicted in Fig. 1c, with non-specific binding determined in the presence of neurotensin (1 µM, Supplementary Fig. 1d) or the $D_3R$ ligand BP897 (50 nM, Supplementary Fig. 1e). After the decay of fluorine-18 (Supplementary Fig. 1a*-e*), the resulting autoradiography of the remaining $^{177}$Lu-labelled binding sites revealed colocalization of NTSR1 and $D_3R$ receptors in the cingulate cortex (Cg), caudate putamen (Cpu) and the islands of Calleja (ICj) of rat brain striatal slices (Fig. 1c).

**Bivalent ligands bind to $D_3R$-NTSR1 with high affinity.** We have recently developed bivalent ligands which are able to recognise $D_2R$-NTSR1 heterodimers with subnanomolar affinity and high selectivity over monomeric $D_2R$ and moderate selectivity over monomeric NTSR1[11]. Chemically, these ligands are composed of a dopamine receptor agonist (*N*-propylindanyl-2-amine) or antagonist (2-methoxy-phenylpiperazine) that is connected to the peptide NTSR1 agonist NT(8-13) by a flexible linker of variable size resulting in the probe molecules **1a-d** and **2a-d**, respectively. This linker consists of a hydrophilic PEG-derived spacer of variable size (22–88 atoms, $m = 1$–4, Fig. 1b) that is connected to the agonist or antagonist pharmacophore through a biphenyltriazole moiety. To investigate whether these bivalent ligands can target $D_3R$-NTSR1 complexes, we performed radioligand binding experiments with membranes from $D_3R$ mono- and $D_3R$-NTSR1 coexpressing HEK293T cells (Supplementary Table 1). In membranes from HEK293T cells expressing only the $D_3R$, all ligands were able to displace [$^3$H]spiperone with $K_i$ values ranging from 0.28 nM to 0.85 nM for compounds **1a-d** and 4.4 nM to 9.5 nM for compounds **2a,c,d**. These affinities are in a similar range to those previously reported for binding to monoexpressed NTSR1[11] (0.24–2.6 nM, Supplementary Table 1). Upon coexpression of $D_3R$ with an excess of NTSR1, the affinity of all compounds strongly increased (relative receptor stoichiometry $D_3R$/NTSR1 1:4, Supplementary Table 1). While the spacer length had no effect on $D_3R$ binding affinity in monoexpressing membranes, the affinity for coexpressing membranes slightly improved with an increasing spacer length. The highest affinities were observed for ligands **1d** and **2d**, displaying $K_i$-values in the one-digit picomolar range (6.1 ± 3.2 pM for **1d**; 4.8 ± 0.8 pM for **2d**, Fig. 2a, b). Due to their lower affinities for monoexpressed $D_3R$, bivalent ligands bearing a dopaminergic antagonist possess higher selectivity for the $D_3R$-NTSR1 coexpressing membranes (**2a, c, d**; 220–1460-fold compared to $D_3R$, 16–170-fold compared to NTSR1) than type **1** bivalent dopamine receptor agonists (**1a-d**; 5.5–140-fold compared to $D_3R$, 22–93 fold compared to NTSR1, Supplementary Table 1). Importantly, coincubation with an excess of NT(8-13) (1 µM) and consequently prevention of a bivalent binding mode by means of a NTSR1-blockade (Supplementary Fig. 2a–c) strongly affected high-affinity binding, leading to $K_i$-values that were comparable to those of $D_3R$ monoexpressing cells (Supplementary Table 1).

It should be noted, that radioligand displacement curves were predominantly monophasic, with more than 90% of binding to the $D_3R$ occurring at very low ligand concentration, if NTSR1 was coexpressed in excess relative to $D_3R$ (4:1 receptor stoichiometry). In contrast, biphasic curves revealing two distinct binding affinities were resolved when membranes from cells expressing an equal amount of NTSR1 and $D_3R$ were used (1:1 receptor stoichiometry, Fig. 2a, b). Under these conditions, 73 ± 1% (**1d**) or 58 ± 1% (**2d**) of radioligand displacement occurred in low
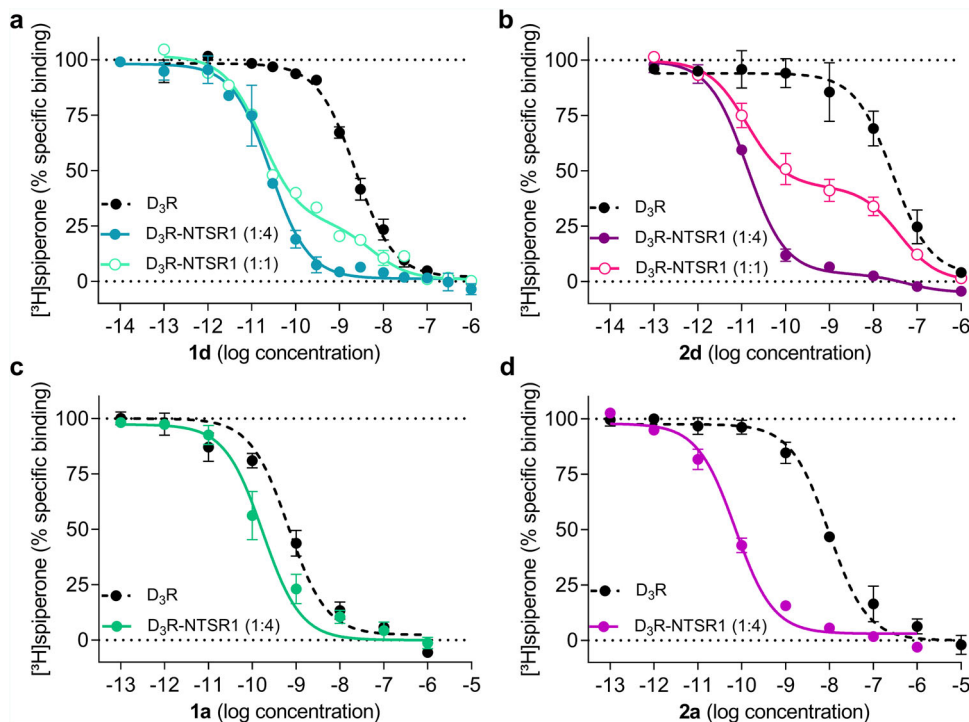
**Fig. 2 D$_3$R Binding behaviour of bivalent ligands.** Competition binding experiments were carried out with [$^3$H]spiperone and membranes from HEK293T cells either monoexpressing D$_3$R or coexpressing D$_3$R and NTSR1. Bivalent ligands **1d** (**a**) and **2d** (**b**) comprising the long 88-atom spacer or **1a** (**c**) and **2a** (**d**) comprising the short 22-atom spacer bind to D$_3$R with binding affinities in the high picomolar to low nanomolar range ($n = 4$ for **1d** and $n = 3$ for **1a**, **2a**, **2d**). Coexpression of an excess of NTSR1 (relative stoichiometry D$_3$R to NTSR1 1:4) results in a 5.5- to 1460-fold increase in affinity ($n = 4$ for **1a**; $n = 5$ for **1d**, **2d** and $n = 3$ for **2a**). Biphasic displacement curves revealing two distinct affinities corresponding to the high- and low-affinity binding mode are resolved when experiments are carried out at a 1:1 D$_3$R to NTSR1 stoichiometry ($n = 3$ for **1d** and **2d**). Data are presented as mean ± s.e.m. of $n$ biologically independent experiments.

picomolar ligand concentration, respectively. This high-affinity binding component was depleted in presence of 1 µM NT(8-13) (Supplementary Fig. 2d), indicating that high-affinity binding is the result of a bivalent D$_3$R-NTSR1 binding mode and low-affinity binding is the result of monovalent engagement of the D$_3$R or NTSR1, respectively.

Interestingly, an increase in D$_3$R-binding affinity upon coexpression of NTSR1 was also observed for compounds **1a** and **2a** comprising a short 22-atom linker (Fig. 2c, d). Similar to ligands with longer spacers, this high-affinity binding was blocked by 1 µM NT(8-13) (Supplementary Fig. 2e). These results are surprising because ligands with such short spacers did not show higher affinity binding to D$_2$R-NTSR1 coexpressing membranes, expected for bivalent binding[11]. This indicates that in contrast to the D$_2$R-NTSR1 dimer, one spacer unit (22 atoms, $m = 1$, Fig. 1b) is sufficient to allow binding to both D$_3$R and NTSR1 protomers of D$_3$R-NTSR1 heterodimers.

**BRET saturation experiments reveal influences of bivalent ligands on D$_3$R-NTSR1 interaction.** In order to directly investigate the effect of ligand binding on the formation of D$_3$R-NTSR1 heterodimers, we performed BRET titration experiments using D$_3$R fused to *Renilla* luciferase (Rluc) and NTSR1 tagged with the mVenus fluorescent protein, in analogy to previous studies investigating the interaction between NTSR1 and D$_2$R.[30,34,37,43] With increasing levels of NTSR1-mVenus expression, a hyperbolic saturation curve was obtained, pointing towards a specific interaction of D$_3$R and NTSR1 (Fig. 3a). Proximity of the two receptors was also observed using in situ proximity ligation assays (PLA)[44] in HEK293T cells transiently transfected with wild-type D$_3$R and NTSR1 (Supplementary

Methods and Supplementary Fig. 3). While preserving the hyperbolic shape of the BRET saturation curve, 1 µM of the monovalent dopamine and neurotensin receptor agonists quinpirole and NT(8-13), respectively, led to a decrease in the maximum BRET signal (BRET$_{max}$, Fig. 3a, b) for the D$_3$R-Rluc/ NTSR1-mVenus complex. In contrast, all bivalent ligands (10 nM) substantially increased BRET$_{max}$ and lowered BRET$_{50}$ and thus promoted the interaction of the two receptors (Figs. 3c, d, 4a, b, Supplementary Fig. 4 and Supplementary Table 2). Similar results were observed when Rluc was exchanged for the brighter and smaller nanoluciferase[45] (Nluc, Supplementary Fig. 5a). The increase in BRET$_{max}$ was most pronounced upon incubation with the bivalent ligands **1d** and **2d** comprising the long 88-atom spacer indicating a linker-dependent effect. Blockade of the D$_3$R by preincubation with high concentrations of the antagonist haloperidol (10 µM, 30 min), and thus inhibition of the bivalent binding mode, completely abolished the effect of the bivalent ligands on BRET$_{max}$ (Figs. 3c and 4a, b). In agreement with previous investigations of D$_2$R-NTSR1 heterodimers[11], bivalent ligands **1a** and **2a** with the short 22-atom spacer did not lead to an enhanced protein-protein interaction in D$_2$R-NTSR1 coexpressing cells. Instead, a decrease in BRET$_{max}$ similar to the effect of monovalent NT(8-13) was observed (Fig. 4c, d). In contrast, incubation with **1a** or **2a** led to an increase in BRET$_{max}$ and a decrease in BRET$_{50}$ in cells expressing NTSR1 together with the D$_3$R subtype (Fig. 4a, b), confirming the selectivity of the short-spacer ligands for the D$_3$R-NTSR1 dimer. Consequently, preincubation with haloperidol had no influence in the D$_2$R-NTSR1 system, while it reverted the effects of the bivalent ligands in the D$_3$R-NTSR1 system (Fig. 4a–d).
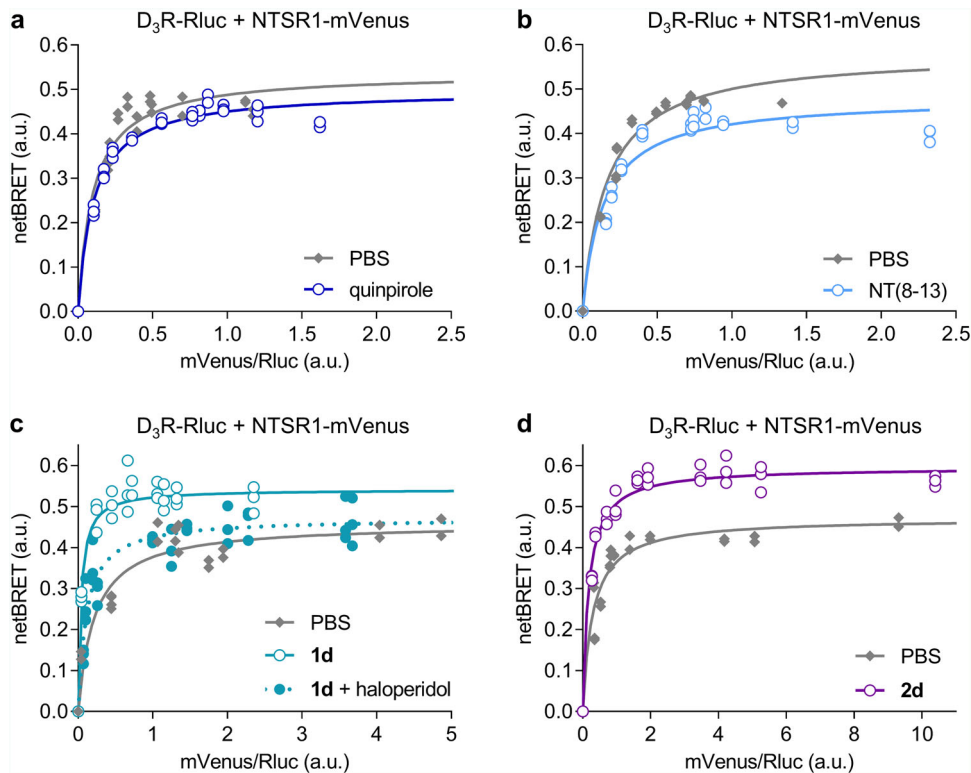
**Fig. 3 BRET Saturation curves are influenced by mono- and bivalent ligands. a, b** The hyperbolic BRET saturation curve for the coexpression of $D_3R$-Rluc and NTSR1-mVenus is indicative of a specific protein–protein interaction. Stimulation of either receptor with monovalent agonists (1 µM) reduces $BRET_{max}$. **c, d** The presence of bivalent ligands (10 nM) strongly increases $BRET_{max}$ and slightly reduces $BRET_{50}$. Preincubation with haloperidol (10 µM, 30 min) abolishes the effect. Data show individual replicates for a single representative experiment of at least three independent repetitions.
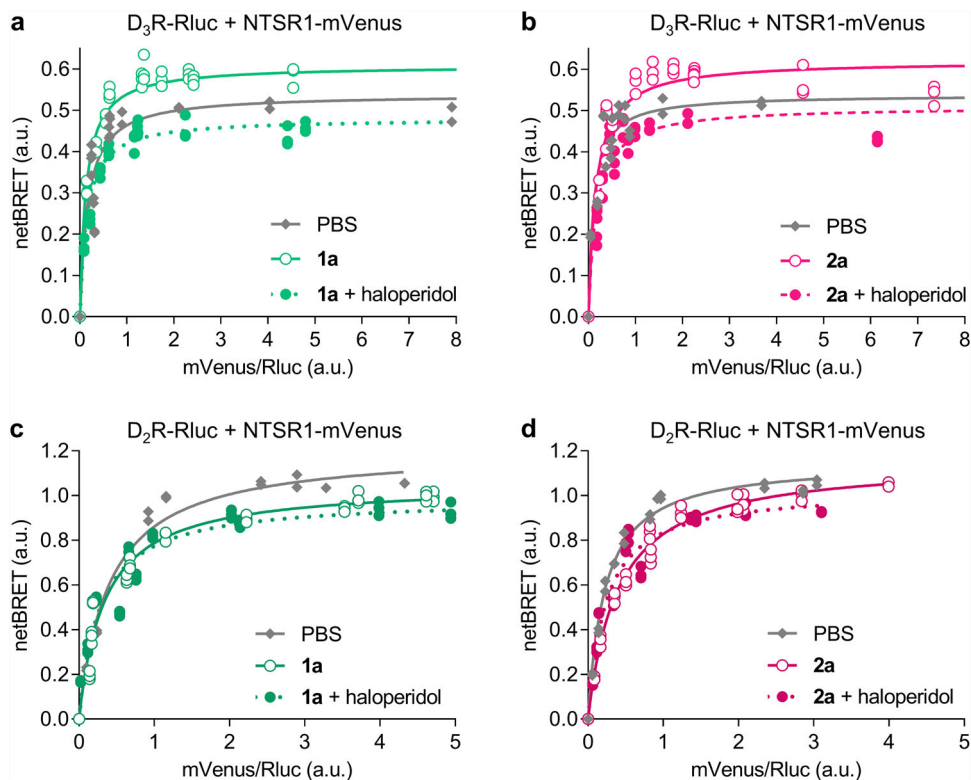


**Fig. 4 Short-spacer bivalent ligands selectively act on $D_3R$-NTSR1. a, b** Bivalent ligands with a 22-atom spacer (**1a, 2a**) increase $BRET_{max}$ between $D_3R$-Rluc and NTSR1-mVenus, but not $D_2R$-Rluc and NTSR1-mVenus (**c, d**). Preincubation with haloperidol (10 µM, 30 min) prevents the effect of the bivalent ligand, resulting in a decrease in $BRET_{max}$ comparable to incubation with NT(8-13) alone. Data show individual replicates for a single representative experiment of at least three independent repetitions.
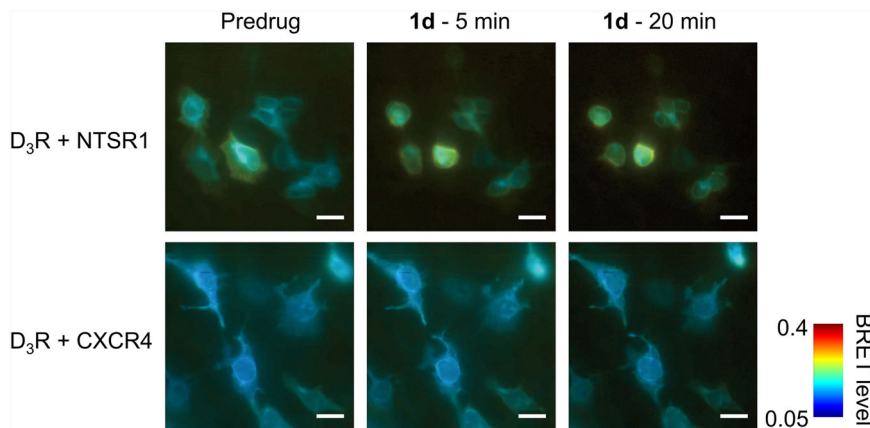
**Fig. 5 BRET imaging of $D_3R$ interaction with NTSR1 compared to CXCR4.** HEK293SL cells were transfected with BRET donor $D_3R$-Nluc and BRET acceptor NTSR1-mVenus or CXCR4-mVenus. 10 µM coelenterazine 400a was added as a substrate. BRET images were obtained before and after the treatment with 10 nM ligand **1d** either for 5 min or 20 min. In each image, BRET levels from 0.05 to 0.4 are expressed as a heat map colour code from blue to red. Adjustments for the correction of the photon counting saturation and Poissonian denoising were applied to the entire images as described in the Methods section. Scale bars, 20 µm. .

BRET displacement experiments[46] with wild-type NTSR1 further confirmed that the effects on $BRET_{max}$ observed in BRET saturation experiments with $D_3R$-Rluc and NTSR1-mVenus are due to changes in the interaction of the two receptors. When an increasing amount of untagged NTSR1 was cotransfected to a constant combination of $D_3R$-Rluc and NTSR1-mVenus, the increase or decrease in $BRET_{max}$ ($\Delta BRET$) induced by 10 nM **1d** or 1 µM NT(8-13), respectively, was diminished, indicating that wild-type NTSR1 competes with NTSR1-mVenus for interaction with $D_3R$-Rluc (Supplementary Fig. 6a). Cotransfection of increasing amounts of CXCR4, a GPCR devoid of specific interactions with $D_3R$[47], does not reduce the effect of the bivalent ligand **1d** (Supplementary Fig. 6b) and has only minor effects on the change in BRET induced by NT(8-13).

Interestingly, we found no differences between type **1** and type **2** ligands, ruling out possible influences of $D_3R$ activation on the BRET saturation assays, since ligands **1a-d** harbour a dopamine agonist pharmacophore whereas type **2** ligands' dopamine pharmacophore is an antagonist. Given that neither chemical inhibition of NTSR1 signalling with the the the $G_{q/11}$ inhibitor YM254890[48] (Supplementary Fig. 5c, d), nor knockout of β-arrestins ($\Delta$β-arrestin HEK cells[49], Supplementary Fig. 5b) affected the ligand-mediated changes in $BRET_{max}$ between $D_3R$-Rluc and NTSR1-mVenus, these are unlikely to result from interference of intracellular signalling proteins. Yet, a potential influence of signal transducers on BRET donors and acceptors cannot be fully excluded, since NTSR1 is known for its promiscuous coupling to various types of G proteins[50].

To investigate the interaction of $D_3R$ and NTSR1 at the single cell level, we performed live-cell BRET imaging[51]. Thus, HEK293SL cells were transfected with $D_3R$-Nluc as the BRET donor and NTSR1-mVenus as the BRET acceptor. After addition of the BRET substrate, an intense BRET signal was observed in cells coexpressing the two receptors. In contrast, coexpression of $D_3R$-Nluc with CXCR4-mVenus resulted in a very weak BRET signal (Fig. 5). Treatment with the bivalent ligand **1d** (10 nM) further increased BRET only for the $D_3R$-NTSR1 coexpressing cells (Fig. 5 and Supplementary Movie 1), which is consistent with the bivalent ligand acting on the $D_3R$-NTSR1 dimer, either by promoting/stabilising the dimer itself or changing the relative receptor conformations. Although it cannot be completely excluded that changes in cell shape occurring upon ligand addition influence the resulting BRET signal, it is unlikely an imaging artefact since BRET is a ratiometric measurement.

**Engaging $D_3R$-NTSR1 heterodimers results in unique $D_3R$ trafficking.** Even though the $D_3R$ possesses high sequence homology with the $D_2R$[12], it is known for its weak interactions with β-arrestins, as well as negligible agonist-induced endocytosis[52,53]. In contrast, functional studies[50] and the recently published cryo-EM structures of the NTSR1-β-arrestin complexes[54,55] leave no doubt about the ability of NTSR1 to recruit β-arrestin and to form a high-affinity complex. To determine the effect of heterodimerization between the $D_3R$ and NTSR1, we investigated β-arrestin recruitment in HEK293 cells stably expressing β-arrestin2 fused to an engineered galactosidase using enzyme fragment complementation (DiscoverX Pathhunter). When the complementary ProLink tag was fused to the C-terminus of $D_3R$ ($D_3R$-ProLink), neither bivalent ligands **1a-d** comprising the agonistic $D_3R$ pharmacophore, nor the reference agonist quinpirole were able to induce detectable β-arrestin2 recruitment in cells expressing only $D_3R$-ProLink (Fig. 6a), although these ligands displayed agonist properties for $D_3R$-mediated G protein activation (Supplementary Fig. 7). When wild-type NTSR1 was coexpressed together with $D_3R$-ProLink, stimulation with monovalent NT(8-13) resulted in a concentration dependent ($EC_{50}$ 1.5 ± 0.4 nM) recruitment of β-arrestin2 indicated by a 2.3-fold increase of the basal luminescence signal (Fig. 6b). It should be noted that in this setup, recruitment of β-arrestin2 to NTSR1 is only detected if it occurs in sufficient proximity to allow for enzyme complementation[11] with the $D_3R$ carrying the ProLink enzyme fragment. When $D_3R$-NTSR1 coexpressing cells were incubated with the bivalent ligands, bell-shaped concentration-response curves were observed. The maximum signal elicited by the bivalent ligands greatly exceeded the response to monovalent NT(8-13). In agreement with the results from the BRET saturation experiments probing dimerization, the effect was most pronounced for compounds with the long 88-atom spacer, **1d** ($E_{max}$ 14-fold of basal luminescence) and **2d** ($E_{max}$ 18-fold of basal luminescence, Fig. 6c,d). Comparison of type **1** and **2** bivalent ligands revealed that the presence of an agonistic $D_3R$ pharmacophore is not required for the induction of β-arrestin2 recruitment, as type **1** bivalent ligands do not show superior efficacy compared to type **2** bivalent ligands comprising the $D_3R$ antagonist. Hence, β-arrestin recruitment is achieved by activation of NTSR1 through the NT(8-13) fragment of the bivalent ligands. Importantly, inhibition of the bivalent binding mode by addition of the $D_3R$ antagonist haloperidol (1 µM) almost completely prevented the
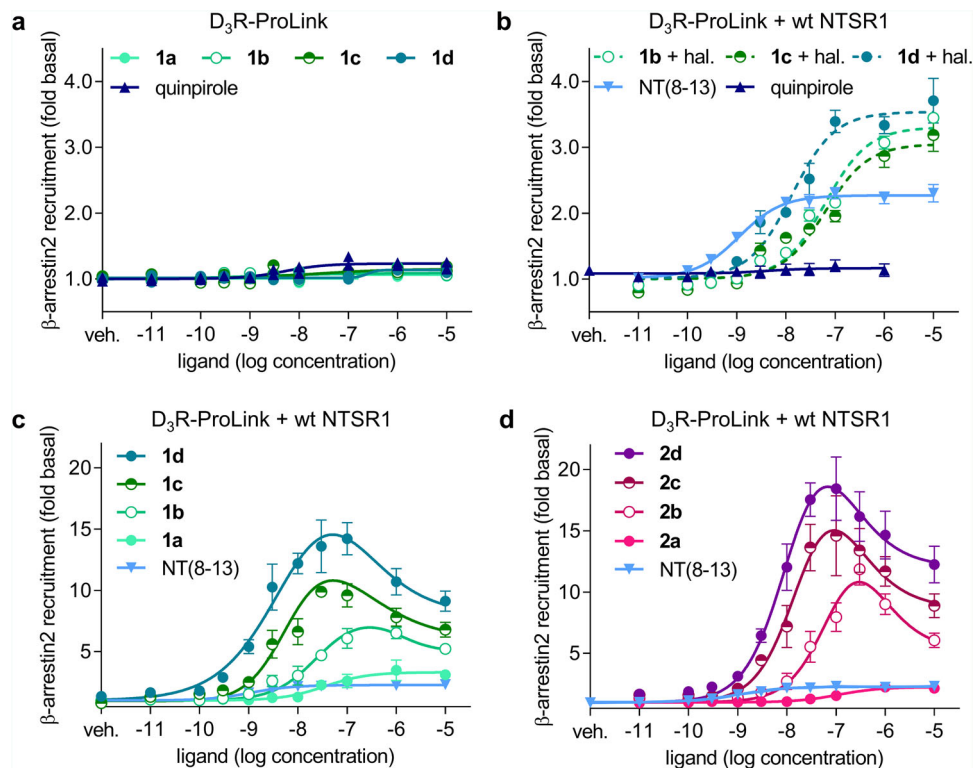
**Fig. 6 β-arrestin2 recruitment to $D_3R$ mono- and $D_3R$-NTSR1 coexpressing HEK293 cells indicates a specific effect of the bivalent ligands.** The DiscoverX enzyme fragment complementation assay allows detection of β-arrestin2 recruitment to a GPCR that is C-terminally tagged with the ProLink fragment. **a** No β-arrestin2 recruitment to $D_3R$-ProLink was detected after stimulation with quinpirole or compounds **1a**-**d** (individual data points, $n = 2$ independent experiments). **b** Coexpression of wild-type NTSR1 does not alter β-arrestin2 recruitment to $D_3R$-Prolink upon stimulation with quinpirole ($n = 3$). NT(8-13) induces a concentration dependent response ($EC_{50}$ 1.5 ± 0.4 nM, $n = 8$). **c, d** Stimulation with type **1** and **2** bivalent ligands results in bell-shaped concentration-response curves in $D_3R$-ProLink-NTSR1 coexpressing cells ($n = 4$ for **1a**-**c**, **2b** and $n = 3$ for **1d**, **2a,c,d**). **b** Prevention of the bivalent binding mode by high concentrations of haloperidol (1 µM, 30 min preincubation, $n = 3$) reduces β-arrestin2 recruitment close to the level of NT(8-13) alone. Error bars denote s.e.m. of $n$ independent experiments.

increase in the maximum effect and abolished the bell-shape, leading to regular concentration-response curves for the bivalent ligands (Fig. 6b). When β-arrestin2 recruitment was investigated with the NTSR1 fused to the ProLink tag (NTSR1-ProLink), the monovalent agonist NT(8-13) was found to strongly induce β-arrestin2 recruitment with a potency in the subnanomolar range ($EC_{50}$ 0.58 ± 0.06 nM, mean ± s.e.m., $n = 8$). Stimulation of NTSR1-ProLink with the bivalent ligands **1b**-**d** and **2b**-**d** also led to sigmoid concentration-response curves with full agonist efficacy, but up to 25-fold lower potency compared to the monovalent agonist NT(8-13) (Supplementary Fig. 8a, b). Similar results were also found using BRET-based arrestin recruitment assays[56] (Supplementary Methods and Supplementary Fig. 8c-f). This is in good agreement with NTSR1-mediated $G_q$ protein activation, where all bivalent ligands showed full agonist efficacy, but were 6–16-fold less potent than NT(8-13) (Supplementary Table 3 and Supplementary Fig. 9a, b). Coexpression of $D_3R$ marginally improved the potency of the bivalent ligands on the $G_q$ response (Supplementary Table 3 and Supplementary Fig. 9c, d).

Application of rGFP targeted to the plasma membrane using a prenylation sequence (CAAX) or to the endosome using a FYVE domain enables quantification of receptor sequestration and internalisation of a GPCR tagged with Rluc by enhanced bystander BRET[56]. In accordance with previous findings[52], we could not detect internalisation of monoexpressed $D_3R$-Rluc after stimulation with 1 µM quinpirole (Fig. 7a, b) or the bivalent ligands **1d** or **2d**, representative for the $D_3R$ agonist or antagonist ligand series (10 nM, Supplementary Fig. 10a, c). In contrast, as

indicated by a decreasing BRET signal between the receptor and rGFP-CAAX and an increasing signal between the receptor and rGFP-FYVE, a strong time-dependent endocytosis of monoexpressed NTSR1-Rluc was observed upon stimulation with NT(8-13) (Fig. 7a, b). Similar to NT(8-13), representative bivalent ligands **1d** and **2d** caused a concentration dependent internalisation of NTSR1 (Supplementary Fig. 10b, d). This is not surprising, since all three ligands share the NT(8-13) substructure. In agreement with earlier findings demonstrating the importance of β-arrestins for internalisation and intracellular trafficking[57], this increase of BRET between rGFP-FYVE and NTSR1-Rluc was completely abolished and the decrease of BRET between rGFP-CAAX and NTSR1-Rluc was strongly diminished, but not absent, in β-arrestin knockout cells (Fig. 7a, b). It is possible that the polybasic sequence of the CAAX-domain does not allow a completely homogenous distribution throughout all compartments of the plasma membrane. Charged residues could impair its diffusion into more ordered hydrophobic regions such as lipid rafts. Stimulation of NTSR1 results in G protein activation, conformational changes and receptor modifications that may lead to receptor sequestration and redistribution to hydrophobic compartments[58] possibly resulting in reduced bystander BRET between NTSR1-Rluc and rGFP-CAAX. Interestingly, bivalent ligands were able to induce $D_3R$ endocytosis, when wild-type NTSR1 was coexpressed with the tagged $D_3R$-Rluc (Fig. 7c, d and Supplementary Fig. 11a, b). Under these conditions, the monovalent agonist quinpirole still did not elicit an effect (Supplementary Fig. 11a, b), while NT(8-13) slightly increased BRET between the receptor and rGFP-FYVE (Fig. 7d and
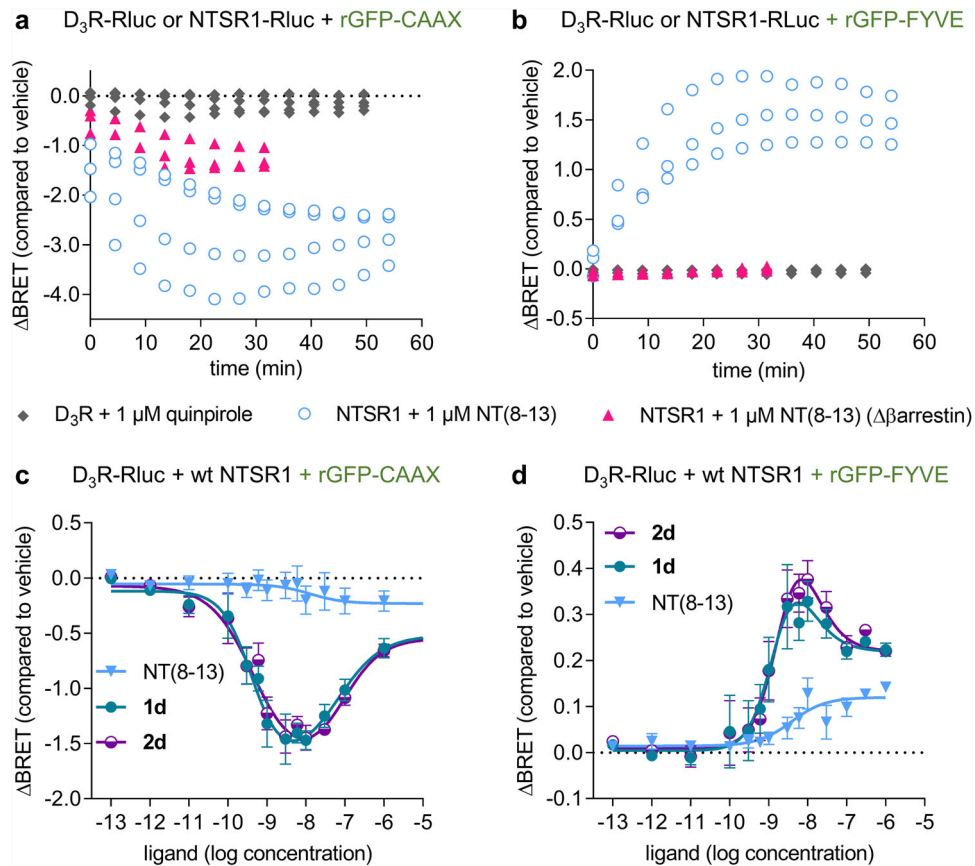
**Fig. 7 Bystander BRET shows the bivalent ligands' ability to induce cointernalization of $D_3R$-NTSR1.** Bystander BRET between $D_3R$-Rluc or NTSR1-Rluc and rGFP-CAAX as membrane marker or rGFP-FYVE as endosome marker is used to monitor receptor trafficking. **a**, **b** Time course of receptor internalisation. Stimulation of NTSR1 with NT(8-13) results in time-dependent sequestration and internalisation as detected by a decreased BRET signal between Rluc and rGFP-CAAX ($n = 4$) and an increased BRET signal between Rluc and rGFP-FYVE ($n = 3$). In cells devoid of β-arrestin1 and β-arrestin2, **a** a small fraction of NTSR1 ($n = 3$) is sequestered from the cell membrane, **b** but does not translocate into FYVE-labelled endosomes ($n = 3$). Internalisation of the $D_3R$ is not observed ($n = 4$). Data are displayed as individual results from biologically independent experiments. **c**, **d** Stimulating $D_3R$-Rluc-NTSR1 coexpressing cells with the bivalent ligands results in $D_3R$ trafficking from the membrane to endosomes. NT(8-13) is able to induce a small increase in the endosomal compartment. Concentration-response curves for $D_3R$ internalisation reveal a bell-shaped profile for bivalent ligands **1d** and **2d** but not for monovalent NT(8-13). Data show mean ± s.e.m. of **c** $n = 6$ and **d** $n = 5$ independent experiments. .

Supplementary Fig. 11b), but did not affect surface BRET between $D_3R$-Rluc and rGFP-CAAX (Fig. 7c and Supplementary Fig. 11a). Concentration-response curves for the bivalent ligands **1d** and **2d** again revealed a bell-shaped concentration-response relationship, with strongly enhanced maximum efficacy compared to NT(8-13) (Fig. 7c, d). Similar to the results from the β-arrestin2 recruitment assays, $D_3R$ cointernalization depended on the spacer length, but not the nature of the $D_3R$ pharmacophore (Supplementary Fig. 11a, b). As for monoexpressed NTSR1, the knockout of β-arrestins strongly diminished the effect of the bivalent ligands on $D_3R$ endocytosis as assessed by coexpressing $D_3R$-Rluc, wild-type NTSR1 and rGFP-CAAX or rGFP-FYVE, emphasising that the internalisation of $D_3R$ is in fact driven by activation and internalisation of NTSR1 (Supplementary Fig. 11c, d). Together these findings are indicative for a specific effect of the bivalent ligands at low ligand concentration. Under these conditions, the ligands simultaneously engage the two protomers of the $D_3R$-NTSR1 complex, enhance the protein-protein interaction and activate NTSR1, thereby leading to internalisation of the trimeric ligand-receptor complex. At higher ligand concentration, monovalent binding prevails and the effect of the bivalent ligands

resembles monomeric NT(8-13), hence explaining the bell-shape of the concentration-response curves.

Results from BRET-based endocytosis assays were confirmed by surface ELISA (Supplementary Methods). As expected, surface expression of monoexpressed NTSR1 was reduced to 56 ± 4% (mean ± s.e.m., $n = 6$) with 1 μM of NT(8-13) and 72 ± 5% (mean ± s.e.m., $n = 5$) with 10 nM of compound **1d**, but not substantially influenced by 1 μM quinpirole (87 ± 6%, mean ± s.e.m., $n = 3$, Supplementary Fig. 12a). Again, treatment with 1 μM of quinpirole, 1 μM of NT(8-13) or 10 nM of bivalent compound **1d** did not lead to apparent changes in surface expression of monoexpressed $D_3R$ (Supplementary Fig. 12b). Upon coexpression of NTSR1, stimulation with NT(8-13) reduced surface expression of the $D_3R$ to 85 ± 6% (mean ± s.e.m., $n = 3$) of the control conditions. Stimulation with the bivalent ligand **1d** led to even stronger internalisation of $D_3R$ in the $D_3R$-NTSR1 coexpressing cells (67 ± 5%, of surface receptor remaining, mean ± s.e.m., $n = 3$, Supplementary Fig. 12c). In agreement with the BRET experiments, the influences on surface expression were abolished in Δβ-arrestin HEK cells (Supplementary Fig. 12d).

## Discussion

Specific interactions of class A GPCRs within the plasma membrane of living cells are capable of modulating the signalling properties, binding affinities and trafficking of the individual receptor protomers[1–6]. While the dimerization of class C GPCRs such as the $GABA_B$ or metabotropic glutamate receptors is compulsory for their expression and function[59], the formation of multimeric class A GPCR complexes is known to be transient[60–63]. Diffusion of class A GPCRs within the membrane can result in random collision or specific interactions of the protomers. Hence, they exist in an equilibrium between monomeric and oligomeric states, which interchange frequently and can be affected through ligand binding[61,64,65]. Bivalent ligands that are composed of two pharmacophores connected by a linker of suitable size are able to engage the binding pockets of two receptors simultaneously. Consequently, bivalent ligands can either recognise a preformed receptor complex, such as a homo- or heterodimer[66], or sequentially bind one protomer and increase the local concentration of the second receptor by binding of the second tethered pharmacophore[7]. Irrespective of the question whether class A GCPR dimerization has functional consequences per se, the mere coexpression of two receptors can be exploited by heterobivalent ligands to harness the thermodynamic advantage of the bivalent binding mode over monovalent binding to either receptor, conferring high affinity and selectivity for the receptor dimer[7,11].

$D_3R$ and NTSR1, two receptors that are involved in various neuropsychiatric diseases and connected to addiction, show overlapping expression in the CNS, especially in the islands of Calleja, a brain region that is connected to reward seeking behaviour[18]. Moreover, neurotensin has been shown to influence $D_3R$ agonist binding in a G protein independent manner in rat brain tissue[38], and $D_3R$ and neurotensin mRNA expression overlap in the rat *nucleus accumbens*, although direct evidence for a cellular colocalization and direct interaction of $D_3R$ and NTSR1 in vivo is pending.

Employing a set of previously described bivalent ligands[11] in binding studies with the radioligand [$^3$H]spiperone, we observed that the coexpression of NTSR1 and $D_3R$ leads to a substantial increase in binding affinity compared to cells that only express $D_3R$ (up to 1460-fold) or NTSR1 (up to 170-fold). This effect depends on the spacer length, leading to one-digit picomolar affinities for ligands **1d** and **2d** with an 88-atom PEG-spacer. The high-affinity binding of the ligands in the $D_3R$-NTSR1 coexpressing cells can be attributed to a bivalent binding mode, as it is abolished in presence of high concentration (1 μM) of monovalent NT(8-13), and the proportion of high- and low-affinity binding sites is affected by the stoichiometry of receptor expression. Compared to the previously reported binding profiles of bivalent ligands to $D_2R$-NTSR1[11], the proportion of high-affinity binding sites reflecting the heterodimer-ligand complex appears to be higher in $D_3R$-NTSR1 coexpressing cells.

BRET-based methods are powerful in detecting and characterising protein-protein interactions[67]. Here we employed BRET saturation experiments and live-cell BRET imaging to study the influence of monovalent and bivalent ligands on the interactions of $D_3R$ and NTSR1. In agreement with previous findings from single molecule tracking experiments describing a prolonged lifetime of $D_2R$ homodimers upon bivalent ligand binding[61], our results indicate that bivalent ligands stabilise the $D_3R$-NTSR1 interaction. This leads to an increased proportion of dimers, regardless of whether a preformed heterodimer is addressed, or if heterodimerization is a bivalent ligand-induced effect. The observation that the increase in $BRET_{max}$ can be

abolished by blocking the $D_3R$ with haloperidol and by titration of wild-type NTSR1 ensures that the observed effects are the result of specific bivalent binding to both receptors. Marsango et al. previously reported reduced levels of $D_3R$ homodimers after incubation with spiperone and haloperidol[68], while an increase in the proportion of $D_2R$ and $D_3R$ homodimers or their lifetime was reported upon incubation with agonists[61,65]. Similar effects seem possible for the $D_3R$-NTSR1 receptor pair, where we observed that binding of monovalent agonists disturbs the heteromeric receptor-receptor interaction.

The bivalent compounds of type **1** and **2** comprise dopaminergic pharmacophores that are not subtype-selective between $D_2R$ and $D_3R$. Based on results from BRET saturation and radioligand binding, bivalent ligands **1a** and **2a** with the short 22-atom spacer ($m = 1$) stabilise $D_3R$-NTSR1 heterodimers, while it was previously described that at least 44-atom-spacers ($m = 2$) are required for bivalent binding to $D_2R$-NTSR1 heterodimers[11]. The individual quaternary structures of the heterodimers allow bivalent ligands to distinguish between $D_3R$-NTSR1 and $D_2R$-NTSR1 heterodimers and may leverage an appealing strategy to design subtype selective ligands without the need for using subtype-selective pharmacophores. Because the dimer-selective binding of **1a** and **2a** over $D_3R$ and NTSR1 monomers is less pronounced compared to their analogs with longer linkers, further optimisation of the linker unit may be of interest for future lead optimisation. Moreover, the combination of $D_3R$-selective pharmacophores with longer linkers may be an interesting alternative for the development of heterobivalent ligands for $D_3R$-NTSR1 with subtype selectivity over $D_2R$-NTSR1.

Previous reports described very weak interactions of the $D_3R$ with β-arrestins and a PKC-mediated clathrin-dependent lysosomal degradation without the involvement of a GRK2/β-arrestin complex[52,69,70]. In accordance with these findings, we observed that while being able to signal through G proteins, mono-expressed $D_3R$ does not recruit β-arrestin2 or internalise upon stimulation with quinpirole. The NTSR1 on the other hand, expectedly recruits β-arrestin2 to the plasma membrane and to endosomes and rapidly internalises upon agonist binding. A luminescence signal resulting from stimulation of NTSR1 with NT(8-13) in $D_3R$-ProLink-NTSR1 coexpressing cells demonstrates that the proximity of the two receptors is sufficient to enable enzyme complementation. Irrespective of the $D_3R$ pharmacophore, bivalent ligands lead to β-arrestin recruitment through activation of the NTSR1 within the heterodimeric complex, with much higher efficacy than the monovalent agonist NT(8-13). If bivalent ligands are used in a concentration range where monovalent binding predominates or if bivalent binding is prevented, β-arrestin recruitment and internalisation of only the NTSR1 occurs. This results in a reduced luminescence output and a reduced bystander BRET as indicated by the decline in the terminal phase of the bell-shaped concentration-response curves. Importantly, the stabilisation of the $D_3R$-NTSR1 heterodimer with the bivalent ligands enables internalisation of a complex consisting of bivalent ligand, $D_3R$, NTSR1 and β-arrestin2, which remains assembled in intracellular compartments. As a result, trafficking of the $D_3R$ is now driven by NTSR1, dramatically changing its pharmacological properties. In a very recent study, a possible link between receptor dimerization, β-arrestin recruitment and internalisation has also been observed for μ-opioid receptors[63].

In agreement with our previous findings on the $D_2R$-NTSR1 heterodimer[11], we could not detect any influences on the signalling properties of the NTSR1 upon coexpressing the $D_3R$ when we investigated β-arrestin2 recruitment and coupling to $G_q$

proteins. It should be noted that under the experimental conditions applied, expression levels of NTSR1 are usually higher than those of $D_3R$. Hence, the presence of monomeric or homodimeric NTSR1 is to be expected, whose signalling may potentially obscure a dimer-specific signalling effect of the bivalent ligands.

Even though the question whether signalling properties of the $D_3R$ change upon reaching intracellular compartments remains elusive, we could successfully demonstrate that bivalent ligands are able to specifically address the $D_3R$ in coexpression with the NTSR1 and that bivalent ligands can shift the trafficking of the $D_3R$ to a β-arrestin mediated endocytosis.

The finding that a class A GPCR-heterodimer can be addressed and stabilised using bivalent ligands to the point that it remains a complex even after internalisation and within intracellular compartments, helps to understand the molecular consequences of receptor dimerization and bivalent ligand binding. Furthermore, it is encouraging and inspiring for the development of novel pharmacological tools, future drugs and innovative therapeutic approaches, in the case of $D_3R$-NTSR1 for example in the field of addiction and substance abuse.

## Methods

**In vitro autoradiography**. Animal experiments were approved by the local animal protection authorities (Government of Central Franconia, Germany, No. 55.2 2532-2-618-14) and performed at the FAU Erlangen-Nürnberg in accordance with the relevant institutional guidelines and EU regulations. The radioligands $^{18}$F-**10** and $^{177}$Lu-**NT127** were synthesised as described previously[39,40] and formulated in saline solution. Coronal rat brain sections (12 μm, female Sprague-Dawley rat (Charles River); strain: Crl:CD(SD)/outbred; age: 22–23 weeks) were cut on a cryostat microtome (HM550, Microm, Germany) and thaw-mounted on covered glass slides (Histobond). The brain slices were carefully dried at room temperature and preincubated for 15 min in assay buffer (50 mM Tris-HCl, 5 mM $MgCl_2$, 50 μg bacitracin, 0.2% BSA, pH 7.4). Afterwards, the sections were incubated in a 50 mL-pot at room temperature for 60 min in assay buffer containing 100 kBq · mL$^{-1}$ $^{18}$F-**10** and/or 20 kBq · mL$^{-1}$ $^{177}$Lu-**NT127** in the presence or absence of BP897 (50 nM) or neurotensin (1 μM). Subsequently, slices were washed three times for 2 min in fresh cold assay buffer and dipped briefly in ice-cold distilled water. The slices were dried under a slight stream of air and exposed to a phosphor imager screen (FUJI Imaging Plate BAS-IP SR) overnight and analysed with a high-resolution radioluminography laser scanner (DÜRR Medical HD-CR 35 Bio, Raytest) to visualise the $^{18}$F-labelled and the $^{177}$Lu-labelled binding sites. After 24 h and complete decay of $^{18}$F, the phosphor imager screen was erased and the slices were again exposed to the imager screen for additional 3 days and again analysed with the high-resolution radioluminography laser scanner to visualise the remaining $^{177}$Lu-labelled binding sites only. Images were created using the software Quantity One (BioRad).

**Cell culture**. HEK293T (ATCC accession number CRL-11268, gift from the Chair of Physiology, FAU Erlangen), HEK293SL[71], Δβ-arrestin-HEK[49] (both donated from Stephane Laporte, Mc Gill University, Montreal, Canada) and HEK293 cells stably expressing β-arrestin2 tagged to the enzyme acceptor (β-arrestin HEK293, DiscoverX) were cultivated in DMEM supplemented with 10% foetal bovine serum (HEK293T, β-arrestin HEK293 and Δβ-arrestin-HEK) or 10% newborn calf serum (HEK293SL), 100 μg · mL$^{-1}$ penicillin, 100 μg · mL$^{-1}$ streptomycin, 2 mM L-glutamine (and 150 μg · mL$^{-1}$ hygromycin for β-arrestin HEK293) at 37 °C and 5% $CO_2$. All cells were regularly confirmed to be free of mycoplasma contamination employing the PCR Mycoplasma Detection Kit (Applied Biological Materials) or luminescence-based MycoAlert Plus Kit (Lonza).

**Plasmids**. Wild-type human $D_3R$ and NTSR1 cDNAs (pcDNA3.1) were obtained from the cDNA resource center (cdna.org). Plasmids (pcDNA3.1) encoding for receptor Rluc8 fusion proteins used in BRET saturation or internalisation assays ($D_3R$-Rluc, NTSR1-Rluc) were constructed in analogy to the previously described $D_{2S}R$-Rluc8 fusion protein[72] employing overlap PCR on the wild-type cDNAs and ligated using the Gibson assembly cloning kit (New England Biolabs). In each case, a 24 amino acid linker (ATGLRSRAQASNSAVDGTAGPVAT) was inserted between the receptor and the luciferase. NTSR1-mVenus has been described previously[34], and the respective $D_3R$-mVenus fusion protein containing the 5 amino acid linker (GGGAS) was cloned in an analogous manner. For the $D_3R$-Nluc construct (pcDNA3.1) used in live-cell BRET imaging, the sequence of the $D_3R$ including the C-terminal 5 amino acid linker (GGGAS) was cloned in frame between the IL6 export signal and the sequence coding for the nanoluciferase enzyme (secretory Nluc, Promega). Plasmids encoding human β-arrestin2-RlucII[73], HA-CXCR4-mVenus (pIRESP)[74], rGFP-CAAX[56] and rGFP-FYVE[56] have been described previously. For enzyme fragment complementation-based readout

of β-arrestin2 recruitment, $D_3R$ was C-terminally tagged with the ARMS2-PK2 sequence in analogy to previously described procedures for $D_{2S}R$[11] and cloned into the pCMV ProLink vector (DiscoverX). For NTSR1-ProLink the cDNA was fused in frame with the PK1 sequence (DiscoverX) in an analogous manner. For ELISA experiments, $D_3R$ N-terminally containing an HA-cleavable sequence and the Flag-Epitope[75], and NTSR1 N-terminally labelled with the 3xHA-epitope (cdna.org) were employed.

**Radioligand binding**. Affinities of the bivalent ligands were determined by radioligand displacement in analogy to previously described protocols[76]. In brief, radioligand binding experiments were carried out using membrane preparations of HEK293T cells transiently monotransfected with $D_3R$ or cotransfected with $D_3R$ and NTSR1 in a cDNA ratio to yield the below mentioned expression levels using polyethylenimine or TransIT293 in a 3:1 ratio of transfection reagent to DNA. We determined an expression level of 540–1400 fmol · mg$^{-1}$ protein ($K_D$ 0.13–0.22 nM) protein for $D_3R$ in the monoexpression system in saturation binding assays using [$^3$H]spiperone (specific acitivity 78.8 Ci · mmol$^{-1}$, Perkin-Elmer, Rodgau, Germany). Membrane preparation with a $D_3R$: NTSR1 ratio of 1:1 comprised 518 fmol · mg$^{-1}$ protein ($K_D$ 0.25 nM) $D_3R$ and 558 fmol · mg$^{-1}$ protein ($K_D$ 0.79 nM) NTSR1, determined with the radioligands [$^3$H]spiperone and [$^3$H] NT(8-13) (specific activity 136 Ci · mmol$^{-1}$, Perkin-Elmer, Rodgau, Germany). Coexpressing membranes with an excess of NTSR1 of at least 4-fold ranged from 200 to 600 fmol · mg$^{-1}$ protein ($K_D$ 0.04–0.24 nM) for $D_3R$ and 1500–7300 fmol · mg$^{-1}$ protein ($K_D$ 0.33–2.3 nM) for NTSR1. Non-specific binding was determined using haloperidol (10 μM for $D_3R$) and NT(8-13) (10 μM for NTSR1). Competition binding experiments were carried out using a protein concentration of 4–18 μg protein per well for the coexpression systems and 1–12 μg per well for the monoexpression system in a total volume of 200 μL. The protein concentration of each membrane preparation was determined by the method of Lowry[77] with bovine serum album (Sigma-Aldrich) as standard. All binding experiments were carried out at 37 °C in binding buffer consisting of 50 mM Tris pH 7.4, 5 nM $MgCl_2$, 1 mM EDTA, 100 μg · mL$^{-1}$ bacitracin and 100 μg · mL$^{-1}$ soybean trypsin inhibitor. Data were normalised to non-specific and total binding and analysed employing one- or two-site competition binding algorithms implemented in GraphPad Prism for windows, version 6.0 (GraphPad Software, San Diego California, USA, www.graphpad.com).

**BRET saturation**. HEK293T cells were detached using Versene (Invitrogen) and diluted to a concentration of 250,000 cells · mL$^{-1}$ in growth medium. Using polyethylenimine (PEI), 300,000 cells were transiently transfected in suspension with a total amount of 1 μg DNA composed of a BRET donor (100 ng $D_{2S}R$-Rluc or 500 ng $D_3R$-Rluc) along with different amounts of BRET acceptor (0–800 ng of NTSR1-mVenus) and complemented to 1 μg with single stranded DNA from salmon testis (ssDNA, Sigma Aldrich). For BRET displacement assays, 300,000 cells per condition were transfected in an analogous manner with 500 ng $D_3R$-Rluc, 100 ng NTSR1-mVenus, 0–150 ng of non-labelled NTSR1 or CXCR4 plasmids, complemented to 1 μg with ssDNA. Cells were seeded in a white 96-well plate (Greiner Bio one) at a density of 25,000 cells per well and cultivated at 37 °C, 5% $CO_2$. After 48 h, the medium was replaced with prewarmed PBS. After 45-60 min at 37 °C, mVenus fluorescence was determined using a CLARIOstar microplate reader (BMG LabTech) with an excitation filter of 497-15 nm and an emission filter of 535-30 nm. Cells were either preincubated for 30 min with 10 μM haloperidol or ligands were added without preincubation in a final concentration of 10 nM (bivalent ligands) or 1 μM (monovalent ligands). After 10 min incubation at room temperature, Colelenterazine-h (Promega, Mannheim, Germany) was added in a final concentration of 5 μM. The BRET$_{ratio}$ was determined after 20 min at room temperature under light exclusion by simultaneous measurement of Rluc and mVenus emission using a filter set of 475-30 nm (donor) and 535-30 nm (acceptor). To determine netBRET, the BRET$_{ratio}$ obtained in the absence of a BRET acceptor was subtracted. NetBRET was plotted against the ratio of mVenus to Rluc counts. Nonlinear regression was performed using the algorithms for one-site specific binding of GraphPad Prism 6.0. For BRET displacement experiments, ΔBRET was calculated as the difference in BRET$_{ratio}$ between the ligand-treated conditions and vehicle-treated controls.

**BRET imaging**. BRET signals were imaged using a BRET microscope composed of an inverted microscope (Eclipse Ti-U, Nikon), an optical filter unit (Lambda 10-2, Sutter Instrument) and an EMCCD camera (HNü512, Nüvü cameras) as described previously[51]. HEK293SL cells were seeded 72 h before the measurement on poly-D-lysine-coated 35 mm glass bottom dishes (P35GC-1.5-14-C, MatTek) at a density of 2–6 × 10$^5$ cells/dish, and transfected at 48 h before the measurement with 100 ng BRET donor (IL6-$D_3R$-GGGAS-Nluc), 400 ng BRET acceptor (NTSR1-mVenus or CXCR4-mVenus) and 500 ng ssDNA using X-tremeGENE 9 transfection reagent (Roche). Just before the imaging experiment, cells were washed with Modified Hank's balanced salt solution (HBSS) (137.9 mM NaCl, 5.33 mM KCl, 1 mM $CaCl_2$, 1 mM $MgCl_2$, 0.44 mM $KH_2PO_4$, 0.33 mM $Na_2HPO_4$, 10 mM HEPES pH 7.4). The bivalent ligand **1d** (10 nM) and the luciferase substrate coelenterazine 400a (10 μM, NanoLight technologies) were diluted with HBSS. Photon counting frames were recorded with EM gain 3000 and 10–100 ms exposure according to the

signal strength. Frames were integrated continuously for 10 s without filter (total luminescence frames), then for 10 s with a band-pass filter (550/80 nm, acceptor frames). Acceptor and total luminescence Images were generated by repeating 15 integration cycles (total exposure time 150 s/channel) and integrating all frames with the same filter settings using MATLAB 2019b. Images were treated with photometric correction[78] and iterative poisson image denoising[79] filters. BRET values were calculated by dividing acceptor counts by total luminescence counts pixelwise, and allocated to 'jet' heatmap array. The movie was generated using ImageJ 1.52a. Frame rate is 5 frames · s$^{-1}$ and frame interval is 60 s.

**β-arrestin2 recruitment**. β-arrestin2 recruitment was investigated employing the Pathhunter assay as described previously[11] and in analogy to the manufacturer's protocol (DiscoverX, Fremont, USA). HEK293 stably expressing β-arrestin2 tagged with the enzyme acceptor (DiscoverX) were transiently transfected using TransIT293 (MoBiTec, Goettingen, Germany). In all, 2 μg of D$_3$R tagged to the ProLink fragment (ARMS2-PK2) either mono- or cotransfected with 0.5 μg of untagged NTSR1. The total amount of receptor was determined by saturation binding experiments to 240 fmol · mg$^{-1}$ protein ($K_D$ 0.43 nM) for the D$_3$R and 4,400 fmol · mg$^{-1}$ protein ($K_D$ 1.4 nM) for the NTSR1. For NTSR1 monoexpression, 0.5 μg NTSR1 tagged with the ProLink fragment (PK1) and 2 μg Mock DNA were transfected and the expression determined to 3,100 fmol · mg$^{-1}$ protein ($K_D$ 1.9 nM). 24 h after transfection, cells were detached using Versene (Invitrogen), resuspended in cell plating reagent 7 (DiscoverX) and seeded in white 384-well plates with clear bottom, (Greiner Bio one) at a density of 5,000 cells per well. After cultivation at 37 °C, 5% CO$_2$ for 24 h, cells were stimulated with the test compounds for 5 h at 37 °C after preincubation with 1 μM YM254890 for 5 min, 1 μM haloperidol for 30 min or without preincubation. 10 μL of the detection mix were added per well chemiluminescence was measured with a CLARIOstar microplate reader after incubation for 60 min in the dark at room temperature. Data were normalised to the basal luminescence and analysed by three-parameter sigmoid or bell-shaped nonlinear regression using the algorithms of GraphPad Prism 6.0.

**BRET internalisation**. HEK293SL cells[71] or Δβ-arrestin-HEK[49] were detached with Trypsin/EDTA (Wisent Inc., St-Bruno, QC, Canada) and 350,000 cells were transiently transfected in suspension using polyethyleneimine. 5 ng of NTSR1-Rluc or 400 ng of D$_3$R-Rluc8 were either mono-or cotransfected with 600 ng of untagged D$_3$R or 5 ng NTSR1, respectively, along with 300 ng rGFP-CAAX or 300 ng rGFP-FYVE and ssDNA to a total of 1 μg DNA. Cells were seeded in white poly-L-ornithine (Sigma Aldrich) coated 96-well plates (Greiner Bio one) at a density of 35,000 cells per well. 48 hours after transfection, cells were washed once with PBS and serum starved for 30–45 min in Tyrode's Buffer at 37 °C, 5% CO$_2$. Coelenterazine-h was added in a final concentration of 3 μM and cells were further incubated at 37 °C, 5% CO$_2$. After 3 min, ligands were added and cells were stimulated for 30 min, 37 °C, 5% CO$_2$ before determining the BRET$_{ratio}$ using a Mithras LB940 multimode microplate reader with 480-20 nm (donor) and 530-20 nm (acceptor) filters. For kinetic experiments, cells were incubated with 3 μM coelenterazine-h for 8 min at 37 °C, 5% CO$_2$., before 1 μM quinpirole or NT(8-13) were added and BRET measurements were immediately started. Ligand-induced effects were monitored by calculation of ΔBRET, which was determined as the difference in BRET$_{ratio}$ between the ligand-treated conditions and vehicle-treated controls. Data were analysed by three-parameter sigmoid or bell-shaped nonlinear regression using the algorithms provided by GraphPad Prism 6.0.

**Statistics and reproducibility**. In general, data are presented as mean ± s.e.m. or mean and individual data points from (n) biologically independent experiments. For the individual experiments, (n) is indicated in the tables and figure legends. For BRET saturation curves, graphs show results from representative experiments, with the individual data points denoting technical replicates. Experiments were repeated at least three times with high reproducibility. Statistical analyses were performed using GraphPad Prism 6.0 and 8.4 for Windows. BRET saturation experiments were analysed using two-tailed, paired Student's $t$ test and $p < 0.05$ was considered as statistically significant (Supplementary Table 2).

**Reporting summary**. Further information on research design is available in the Nature Research Reporting Summary linked to this article.

## Data availability
The data that support the findings of this study are available within the Supplementary Information, source data for Figs. 2–4, 6 and 7 is available as Supplementary Data 1 and/ or from the corresponding authors upon reasonable request.

## References

1.  Bouvier, M. Oligomerization of G-protein-coupled transmitter receptors. *Nat. Rev. Neurosci.* **2**, 274–286 (2001).
2.  Han, Y., Moreira, I. S., Urizar, E., Weinstein, H. & Javitch, J. A. Allosteric communication between protomers of dopamine class A GPCR dimers modulates activation. *Nat. Chem. Biol.* **5**, 688–695 (2009).
3.  Jordan, B. A. & Devi, L. A. G-protein-coupled receptor heterodimerization modulates receptor function. *Nature* **399**, 697–700 (1999).
4.  Terrillon, S., Barberis, C. & Bouvier, M. Heterodimerization of V1a and V2 vasopressin receptors determines the interaction with β-arrestin and their trafficking patterns. *Proc. Natl Acad. Sci. USA* **101**, 1548–1553 (2004).
5.  White, J. F. et al. Dimerization of the class A G protein-coupled neurotensin receptor NTS1 alters G protein interaction. *Proc. Natl Acad. Sci. USA* **104**, 12199–12204 (2007).
6.  Botta, J., Appelhans, J. & McCormick, P. J. Continuing challenges in targeting oligomeric GPCR-based drugs. *Prog. Mol. Biol. Transl. Sci.* **169**, 213–245 (2020).
7.  Hiller, C., Kühhorn, J. & Gmeiner, P. Class A G-protein-coupled receptor (GPCR) dimers and bivalent ligands. *J. Med. Chem.* **56**, 6542–6559 (2013).
8.  Daniels, D. J., Kulkarni, A., Xie, Z., Bhushan, R. G. & Portoghese, P. S. A bivalent ligand (KDAN-18) containing δ-antagonist and κ-agonist pharmacophores bridges δ2 and κ1 opioid receptor phenotypes. *J. Med. Chem.* **48**, 1713–1716 (2005).
9.  Shonberg, J., Scammells, P. J. & Capuano, B. Design strategies for bivalent ligands targeting GPCRs. *ChemMedChem* **6**, 963–974 (2011).
10. Waldhoer, M. et al. A heterodimer-selective agonist shows in vivo relevance of G protein-coupled receptor dimers. *Proc. Natl Acad. Sci. USA* **102**, 9050–9055 (2005).
11. Hübner, H. et al. Structure-guided development of heterodimer-selective GPCR ligands. *Nat. Commun.* **7**, 12298 (2016).
12. Sokoloff, P., Giros, B., Martres, M. P., Bouthenet, M. L. & Schwartz, J. C. Molecular-cloning and characterization of a novel dopamine receptor (D3) as a target for neuroleptics. *Nature* **347**, 146–151 (1990).
13. Joyce, J. N. & Millan, M. J. Dopamine D3 receptor antagonists as therapeutic agents. *Drug Discov. Today* **10**, 917–925 (2005).
14. Yang, P., Perlmutter, J. S., Benzinger, T. L. S., Morris, J. C. & Xu, J. Dopamine D3 receptor: A neglected participant in Parkinson disease pathogenesis and treatment? *Ageing Res. Rev.* **57**, 100994 (2020).
15. Montoya, A. et al. Dopamine receptor D3 signalling in astrocytes promotes neuroinflammation. *J. Neuroinflammation* **16**, 258–258 (2019).
16. Levant, B. Differential distribution of D3 dopamine receptors in the brains of several mammalian species. *Brain Res.* **800**, 269–274 (1998).
17. Levesque, D. et al. Identification, characterization, and localization of the dopamine D3 receptor in rat brain using 7-[$^3$H]hydroxy-N,N-di-n-propyl-2-aminotetralin. *Proc. Natl Acad. Sci. USA* **89**, 8155–8159 (1992).
18. Ikemoto, S. Dopamine reward circuitry: two projection systems from the ventral midbrain to the nucleus accumbens–olfactory tubercle complex. *Brain Res. Rev.* **56**, 27–78 (2007).
19. Le Foll, B. et al. Dopamine D3 receptor ligands for drug addiction treatment: update on recent findings. *Prog. Brain Res.* **211**, 255–275 (2014).
20. Sokoloff, P. & Le Foll, B. The dopamine D3 receptor, a quarter century later. *Eur. J. Neurosci.* **45**, 2–19 (2017).
21. Heidbreder, C. A. & Newman, A. H. Current perspectives on selective dopamine D3 receptor antagonists as pharmacotherapeutics for addictions and related disorders. *Ann. N. Y. Acad. Sci.* **1187**, 4–34 (2010).
22. Newman, A. H., Grundt, P. & Nader, M. A. Dopamine D3 receptor partial agonists and antagonists as potential drug abuse therapeutic agents. *J. Med. Chem.* **48**, 3663–3679 (2005).
23. Sarrieau, A. et al. Characterization and autoradiographic distribution of neurotensin binding sites in the human brain. *Brain Res.* **348**, 375–380 (1985).
24. Boudin, H., Pélaprat, D., Rostène, W. & Beaudet, A. Cellular distribution of neurotensin receptors in rat brain: immunohistochemical study using an antipeptide antibody against the cloned high affinity receptor. *J. Comp. Neurol.* **373**, 76–89 (1996).

25. Sarret, P. & Cavelier, F. *Neurotensin and Its Receptors in Reference Module in Neuroscience and Biobehavioral Psychology* (Elsevier, 2017).

26. Dobbs, L. K. & Morikawa, H. Biasing neurotensin receptor signaling to arrest psychostimulant abuse. *Cell* **181**, 1205–1206 (2020).

27. Barak, L. S. et al. ML314: a biased neurotensin receptor ligand for methamphetamine abuse. *ACS Chem. Biol.* **11**, 1880–1890 (2016).

28. Slosky, L. M. et al. β-Arrestin-biased allosteric modulator of NTSR1 selectively attenuates addictive behaviors. *Cell* **181**, 1364–1379.e1314 (2020).

29. Dijkman, P. M. et al. Dynamic tuneable G protein-coupled receptor monomer-dimer populations. *Nat. Commun.* **9**, 1710 (2018).

30. Borroto-Escuela, D. O. et al. Dopamine D2 receptor signaling dynamics of dopamine D2-neurotensin 1 receptor heteromers. *Biochem. Biophys. Res. Commun.* **435**, 140–146 (2013).

31. Koschatzky, S., Tschammer, N. & Gmeiner, P. Cross-receptor interactions between dopamine D2L and neurotensin NTS1 receptors modulate binding affinities of dopaminergics. *ACS Chem. Neurosci.* **2**, 308–316 (2011).

32. Perron, A., Sharif, N., Sarret, P., Stroh, T. & Beaudet, A. NTS2 modulates the intracellular distribution and trafficking of NTS1 via heterodimerization. *Biochem. Biophys. Res. Commun.* **353**, 582–590 (2007).

33. Hwang, J. R. et al. Intermolecular cross-talk between NTR1 and NTR2 neurotensin receptor promotes intracellular sequestration and functional inhibition of NTR1 receptors. *Biochem. Biophys. Res. Commun.* **391**, 1007–1013 (2010).

34. Plach, M. et al. Differential allosteric modulation within dopamine D2R—neurotensin NTS1R and D2R—serotonin 5-HT2AR receptor complexes gives bias to intracellular calcium signalling. *Sci. Rep.* **9**, 16312 (2019).

35. Binder, E. B., Kinkead, B., Owens, M. J. & Nemeroff, C. B. Neurotensin and dopamine interactions. *Pharmacol. Rev.* **53**, 453–486 (2001).

36. Diaz, J. et al. Opposing roles for dopamine D2 and D3 receptors on neurotensin mRNA expression in nucleus accumbens. *Eur. J. Neurosci.* **6**, 1384–1387 (1994).

37. Koschatzky, S. & Gmeiner, P. Selective agonists for dopamine/neurotensin receptor heterodimers. *ChemMedChem* **7**, 509–514 (2012).

38. Liu, Y., Hillefors-Berglund, M. & von Euler, G. Modulation of dopamine D3 receptor binding by N-ethylmaleimide and neurotensin. *Brain Res.* **643**, 343–348 (1994).

39. Fehler, S. K. et al. Fast and efficient $^{18}$F-labeling by [$^{18}$F]fluorophenylazocarboxylic esters. *Chem. Eur. J.* **20**, 370–375 (2014).

40. Maschauer, S. et al. In vivo monitoring of the antiangiogenic effect of neurotensin receptor-mediated radiotherapy by small-animal positron emission tomography: a pilot study. *Pharmaceuticals* **7**, 464–481 (2014).

41. Stanwood, G. D., Lucki, I. & McGonigle, P. Differential regulation of dopamine D2 and D3 receptors by chronic drug treatments. *J. Pharmacol. Exp. Ther.* **295**, 1232–1240 (2000).

42. Betancur, C. et al. Characterization of binding sites of a new neurotensin receptor antagonist, [$^3$H]SR 142948A, in the rat brain. *Eur. J. Pharmacol.* **343**, 67–77 (1998).

43. Ullmann, T. et al. Homobivalent dopamine D2 receptor ligands modulate the dynamic equilibrium of D2 monomers and homo- and heterodimers. *ACS Chem. Biol.* **16**, 371–379 (2021).

44. Gomes, I., Sierra, S. & Devi, L. A. Detection of receptor heteromerization using in situ proximity ligation assay. *Curr. Protoc. Pharmacol.* **75**, 2.16.11–12.16.31 (2016).

45. Hall, M. P. et al. Engineered luciferase reporter from a deep sea shrimp utilizing a novel imidazopyrazinone substrate. *ACS Chem. Biol.* **7**, 1848–1857 (2012).

46. Borroto-Escuela, D. O., Flajolet, M., Agnati, L. F., Greengard, P. & Fuxe, K. Bioluminescence resonance energy transfer methods to study G protein-coupled receptor-receptor tyrosine kinase heteroreceptor complexes. *Methods Cell Biol.* **117**, 141–164 (2013).

47. Marcellino, D. et al. Identification of dopamine D1–D3 receptor heteromers: indications for a role of synergistic D1–D3 receptor interactions in the striatum. *J. Biol. Chem.* **283**, 26016–26025 (2008).

48. Peng, Q. & Shen, J. YM-254890 is a general inhibitor of G proteins. *FASEB J.* **33**, 503.507–503.507 (2019).

49. Cahill, T. J. et al. Distinct conformations of GPCR–β-arrestin complexes mediate desensitization, signaling, and endocytosis. *Proc. Natl Acad. Sci. USA* **114**, 2562–2567 (2017).

50. Besserer-Offroy, É. et al. The signaling signature of the neurotensin type 1 receptor with endogenous ligands. *Eur. J. Pharmacol.* **805**, 1–13 (2017).

51. Kobayashi, H., Picard, L.-P., Schönegge, A.-M. & Bouvier, M. Bioluminescence resonance energy transfer–based imaging of protein–protein interactions in living cells. *Nat. Protoc.* **14**, 1084–1107 (2019).

52. Kim, K.-M. et al. Differential regulation of the dopamine D2and D3 receptors by G protein-coupled receptor kinases and β-arrestins. *J. Biol. Chem.* **276**, 37409–37414 (2001).

53. Kim, K.-M., Gainetdinov, R. R., Laporte, S. A., Caron, M. G. & Barak, L. S. G Protein-coupled receptor kinase regulates dopamine D3 receptor signaling by modulating the stability of a receptor-filamin-β-arrestin complex: a case of autoreceptor regulation. *J. Biol. Chem.* **280**, 12774–12780 (2005).

54. Yin, W. et al. A complex structure of arrestin-2 bound to a G protein-coupled receptor. *Cell Res.* **29**, 971–983 (2019).

55. Huang, W. et al. Structure of the neurotensin receptor 1 in complex with β-arrestin 1. *Nature* **579**, 303–308 (2020).

56. Namkung, Y. et al. Monitoring G protein-coupled receptor and beta-arrestin trafficking in live cells using enhanced bystander BRET. *Nat. Commun.* **7**, 12178 (2016).

57. Oakley, R. H., Laporte, S. A., Holt, J. A., Barak, L. S. & Caron, M. G. Molecular determinants underlying the formation of stable intracellular G protein-coupled receptor-β-arrestin complexes after receptor endocytosis. *J. Biol. Chem.* **276**, 19452–19460 (2001).

58. Heakal, Y. & Kester, M. Nanoliposomal short-chain ceramide inhibits agonist-dependent translocation of neurotensin receptor 1 to structured membrane microdomains in breast cancer cells. *Mol. Cancer Res.* **7**, 724 (2009).

59. Chun, L., Zhang, W.-h & Liu, J.-f Structure and ligand recognition of class C GPCRs. *Acta Pharmacol. Sin.* **33**, 312–323 (2012).

60. Hern, J. A. et al. Formation and dissociation of M1 muscarinic receptor dimers seen by total internal reflection fluorescence imaging of single molecules. *Proc. Natl Acad. Sci. USA* **107**, 2693–2698 (2010).

61. Tabor, A. et al. Visualization and ligand-induced modulation of dopamine receptor dimerization at the single molecule level. *Sci. Rep.* **6**, 33233 (2016).

62. Calebiro, D. et al. Single-molecule analysis of fluorescently labeled G-protein–coupled receptors reveals complexes with distinct dynamics and organization. *Proc. Natl Acad. Sci. USA* **110**, 743–748 (2013).

63. Möller, J. et al. Single-molecule analysis reveals agonist-specific dimer formation of μ-opioid receptors. *Nat. Chem. Biol.* **16**, 946–954 (2020).

64. Cheng, Z.-J. & Miller, L. J. Agonist-dependent dissociation of oligomeric complexes of G protein-coupled cholecystokinin receptors demonstrated in living cells using bioluminescence resonance energy transfer. *J. Biol. Chem.* **276**, 48040–48047 (2001).

65. Kasai, R. S., Ito, S. V., Awane, R. M., Fujiwara, T. K. & Kusumi, A. The class-A GPCR dopamine D2 receptor forms transient dimers stabilized by agonists: detection by single-molecule tracking. *Cell Biochem. Biophys.* **76**, 29–37 (2018).

66. Busnelli, M. et al. Design and characterization of superpotent bivalent ligands targeting oxytocin receptor dimers via a channel-like structure. *J. Med. Chem.* **59**, 7152–7166 (2016).

67. Hamdan, F. F., Percherancier, Y., Breton, B. & Bouvier, M. Monitoring protein-protein interactions in living cells by bioluminescence resonance energy transfer (BRET). *Curr. Protoc. Neurosci.* **34**, 5.23.21–25.23.20 (2006).

68. Marsango, S. et al. A molecular basis for selective antagonist destabilization of dopamine D3 receptor quaternary organization. *Sci. Rep.* **7**, 2134 (2017).

69. Zhang, X., Sun, N., Zheng, M. & Kim, K.-M. Clathrin-mediated endocytosis is responsible for the lysosomal degradation of dopamine D3 receptor. *Biochem. Biophys. Res. Commun.* **476**, 245–251 (2016).

70. Cho, E.-Y. et al. Roles of protein kinase C and actin-binding protein 280 in the regulation of intracellular trafficking of dopamine D3 receptor. *Mol. Endocrinol.* **21**, 2242–2254 (2007).

71. Robertson, D. N. et al. Design and construction of conformational biosensors to monitor ion channel activation: a prototype FlAsH/BRET-approach to Kir3 channels. *Methods* **92**, 19–35 (2016).

72. Guo, W. et al. Dopamine D2 receptors form higher order oligomers at physiological expression levels. *EMBO J.* **27**, 2293–2304 (2008).

73. Quoyer, J. et al. Pepducin targeting the C-X-C chemokine receptor type 4 acts as a biased agonist favoring activation of the inhibitory G protein. *Proc. Natl Acad. Sci. USA* **110**, E5088–E5097 (2013).

74. Paradis, J. S. et al. Receptor sequestration in response to β-arrestin-2 phosphorylation by ERK1/2 governs steady-state levels of GPCR cell-surface expression. *Proc. Natl Acad. Sci. USA* **112**, E5160–E5168 (2015).

75. Guan, X. M., Kobilka, T. S. & Kobilka, B. K. Enhancement of membrane insertion and function in a type IIIb membrane protein following introduction of a cleavable signal peptide. *J. Biol. Chem.* **267**, 21995–21998 (1992).

76. Hübner, H., Haubmann, C., Utz, W. & Gmeiner, P. Conjugated enynes as nonaromatic catechol bioisosteres: synthesis, binding experiments and computational studies of novel dopamine receptor agonists recognizing preferentially the D3 subtype. *J. Med. Chem.* **43**, 756–762 (2000).

77. Lowry, O. H., Rosebrough, N. J., Farr, A. L. & Randall, R. J. Protein measurement with the folin phenol reagent. *J. Biol. Chem.* **193**, 265–275 (1951).

78. Basden, A. G., Haniff, C. A. & Mackay, C. D. Photon counting strategies with low-light-level CCDs. *Mon. Not. R. Astron. Soc.* **345**, 985–991 (2003).

79. Azzari, L. & Foi, A. Variance stabilization for noisy+estimate combination in iterative poisson denoising. *IEEE Signal Process. Lett.* **23**, 1086–1090 (2016).

## Author contributions

J.B. performed and analysed BRET and radioligand binding experiments with assistance from P.C., H.V. and H.K.; S.M. and O.P. performed radiosynthesis and autoradiography and analysed the data. J.B. and H.V. performed and analysed in situ PLA experiments. H.K. performed and analysed live-cell BRET imaging. P.G. contributed bivalent ligands. A.R. contributed precursors for radiosynthesis. M.B. and D.W. conceived the experiments, were responsible for the overall project strategy and provided project supervision. J.B., M.B. and D.W. wrote the manuscript with contributions from all authors. All authors have approved the final version of the manuscript.

## Competing interests

The authors declare the following competing interests: some of the biosensors used in this study were licensed to Domain Therapeutics for commercial use but are freely available for academic research upon request. M.B. is the president of the scientific advisory board of Domain Therapeutics. The remaining authors declare no competing interests.

## Additional information

**Supplementary information** The online version contains supplementary material available at https://doi.org/10.1038/s42003-021-02574-4.

**Correspondence** and requests for materials should be addressed to Michel Bouvier or Dorothee Weikert.

**Peer review information** *Communications Biology* thanks Elizabeth Johnstone, Martina Kocan and the other, anonymous, reviewers for their contribution to the peer review of this work. Primary Handling Editors: Ross Bathgate and Christina Karlsson Rosenthal.

**Reprints and permission information** is available at http://www.nature.com/reprints

**Publisher's note** Springer Nature remains neutral with regard to jurisdictional claims in published maps and institutional affiliations.